Mutant and Wild-Type Myoglobin-CO Protein Dynamics: Vibrational Echo Experiments

K. D. Rector,[†] C. W. Rella,[‡] Jeffrey R. Hill,[§] A. S. Kwok,[†] Stephen G. Sligar,[§] Ellen Y. T. Chien,[§] Dana D. Dlott,*[,§] and M. D. Fayer*[,†]

Department of Chemistry, Stanford University, Stanford, California 94305, Stanford Free Electron Laser Center, Hansen Experimental Physics Laboratory, Stanford University, Stanford, California 94305-4085, and School of Chemical Sciences, University of Illinois at Urbana−Champaign, Urbana, Illinois 61801

Received: October 18, 1996; In Final Form: December 19, 1996[⊗]

Picosecond infrared vibrational echo experiments on a mutant protein, H64V myoglobin-CO, are described and compared to experiments on wild-type myoglobin-CO. H64V is myoglobin with the distal histidine replaced by a valine. The vibrational dephasing experiments examine the influence of protein dynamics on the CO ligand, which is bound to the active site of the mutant protein, from low temperature to physiologically relevant temperatures. The experiments were performed with a mid-infrared free electron laser tuned to the CO stretch mode at 1969 cm^{-1}. The vibrational echo results are combined with infrared pump−probe measurements of the CO vibrational lifetime to yield the homogeneous pure dephasing. The homogeneous pure dephasing is the Fourier transform of the homogeneous line width with the lifetime contribution removed. The measurements were made from 60 to 300 K and show that the CO vibrational spectrum is inhomogeneously broadened at all temperatures studied. The mutant protein's CO vibrational pure dephasing rate is ∼20% slower (narrower homogeneous pure dephasing line width) than the wild-type protein at all temperatures, although the only difference between the two proteins is the replacement of the wild-type's polar distal histidine amino acid by a nonpolar valine. These results provide insights into the mechanisms of the transmission of protein fluctuations to the CO ligand bound at the active site, and they are consistent with previously proposed mechanisms of protein−ligand coupling.

Introduction

Myoglobin (Mb), the oxygen carrier in muscle, is a single polypeptide chain of 153 amino acids and has a mass of 18 kD.[1] The capacity of myoglobin to bind oxygen, carbon monoxide, and other ligands depends on the presence of a non-polypeptide prosthetic group protoheme [Fe(II)protoporphyrin IX]. The interior of the protein consists almost entirely of nonpolar amino acids, while the exterior part of the protein contains both polar and nonpolar residues. The only internal polar amino acids are two histidines.[1] As shown in Figure 1, the proximal histidine is covalently bonded to the Fe, forming the fifth coordination site of the heme. The sixth coordinate site of the heme is the active site of the protein where the ligand bonds. The distal histidine is physically near the sixth coordinate site of the heme but not directly covalently bonded to it. This paper presents a study of a mutant of wild-type sperm whale myoglobin and a comparison of it to myoglobin. Wild-type sperm whale Mb is different from native sperm whale Mb only in the addition of a methionine residue near the n-terminus. Both the wild-type and the mutant have this extra amino acid.

When bound to Mb, the CO vibrational frequency is substantially red-shifted from the gas-phase frequency and separated into several distinct bands, which are labeled A_0-A_3 in order of decreasing carbonyl frequency. Although the intensities and widths of these bands are sensitive to temperature, pressures, and pH, the peak frequencies remain largely unchanged.[2] These four bands, which occur at 1969, 1945, 1942, and 1930 cm^{-1}, reflect distinct conformational substates and are believed to arise because of the distinct through-space electric field perturbations caused by the $H^{\epsilon 2} \leftrightarrow H^{\delta 1}$ tautomerism and a 180° $C^{\beta}-C^{\gamma}$ ring flip of the distal histidine residue.[3] Other models have suggested hydrogen bonding or steric interactions.

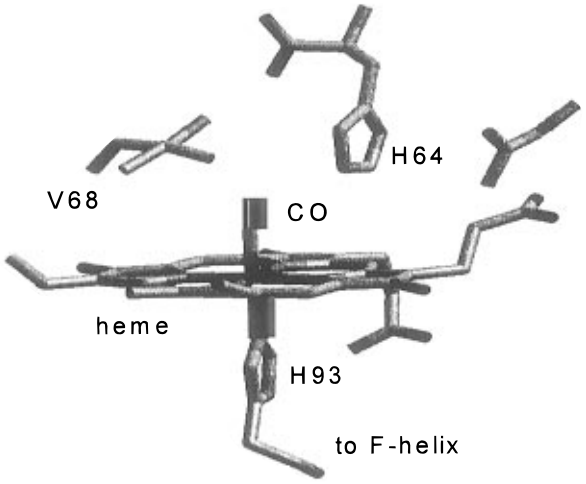

Figure 1. Myoglobin-CO in the vicinity of the heme adapted from Yang and Phillips.[48] The distal histidine is labeled H64 and the proximal histidine is labeled H93. The CO is bound to the heme and coupled to the extensively delocalized heme electrons.

A substantial literature exists that explores the structure and binding kinetics of CO at the active site of Mb using a variety of techniques, including X-ray crystallography,[4,5] ^{13}C NMR,[3] time-dependent optical spectroscopy,[6−9] Raman spectroscopy,[10,11] and mid-infrared absorption spectroscopy.[2,12,13] While these methods yield a wealth of information about the equilibrium structure of Mb−CO and the CO binding kinetics, they provide only indirect dynamical information about the protein with a ligand bound to the active site. Molecular dynamics simulations show that Mb has a flexible structure in constant

[†] Department of Chemistry, Stanford University.
[‡] Stanford Free Electron Laser Center.
[§] University of Illinois at Urbana−Champaign.
* Corresponding authors.
[⊗] Abstract published in *Advance ACS Abstracts,* February 1, 1997.

S1089-5647(96)03226-9 CCC: $14.00

motion at room temperature.[14] Such motions can be either on a relatively small scale involving a few of the constituent atoms, such as the torsion of an amino acid residue, or they can be large-scale motions involving entire regions of the protein backbone. Simulations over a period of 300 ps indicate that Mb samples thousands of local energy minima of approximately equal energies, separated by barriers of varying height.[14] These minima correspond to different conformational substates of the protein. It has been proposed that this characteristic of proteins is analogous to the energy landscape in glasses.[15]

Recently, the first picosecond infrared vibrational echo experiments[16] on a biological system, myoglobin-CO, were reported.[17,18] Vibrational echo studies were performed on the CO stretch A_1 line. Pure dephasing is the rate of coherence loss of an ensemble of vibrational transitions with contributions from inhomogeneous broadening and population relaxation (T_1) removed. The rate of pure dephasing, $1/T_2^*$ was measured from 60 to 300 K. The temperature-dependent pure dephasing rate has a functional form that can be described as a power law plus an exponentially activated process:

$$1/T_2^* = aT^{\alpha} + be^{-\Delta E/kT} \tag{1}$$

where T_2^* is the pure dephasing time constant, T is temperature, α is the power law exponent, ΔE is the activation energy, and k is Boltzmann's constant. Below the glass transition temperature of the glycerol/water (95:5; v:v) solvent, $T_g \sim 185$ K, the data were described by the power law, and the exponent of the power law is $\alpha = 1.3 \pm 0.1$. A distinct break in the slope of the temperature dependence around T_g is observed. Above T_g, $\Delta E \cong 1000$ cm^{-1}.

The vibrational echo studies provided insights into how protein dynamics couple to the ligand bound at the protein's active site. A number of fundamental issues are addressed: What is the mechanism that couples the protein fluctuations to the CO stretching frequency, causing the pure dephasing? Why is there a change in the nature of the dynamics near T_g? And, how does protein structure influence dynamics experienced at the active site?

To more fully understand the nature of protein dynamics communicated to the active site in Mb, we performed a detailed temperature-dependent vibrational echo study of a mutant of Mb in which the polar distal histidine is replaced with nonpolar valine (H64V). Changes in the magnitude of the pure dephasing of the mutant provide insights into the coupling mechanism. In this paper, the vibrational echo studies of the CO dephasing of H64V are compared to the previous studies on Mb−CO.[17] The results show that replacing the distal histidine with valine is a sufficient modification of the protein to change the CO vibrational dephasing over the entire temperature range. The vibrational dephasing rate of the mutant is smaller than that of Mb but has an identical temperature dependence within experimental error. The current experiments are discussed in terms of the model proposed in the context of the Mb results.[17]

Vibrational Echo Method and Experimental Procedures

Vibrational line shapes in condensed phases contain the details of the dynamic interactions of a normal mode with its environment.[19−21] However, the line shape can also include essentially static, structural perturbations associated with the distribution of local configurations of the environment of the vibrational oscillator, i.e., inhomogeneous broadening. The IR absorption or Raman line shape represents a convolution of the various dynamic and static contributions.[22] The picosecond infrared vibrational echo experiment is a time domain, nonlinear method that can extract the homogeneous vibrational line shape from an inhomogeneously broadened line.[16,23] By combining vibrational echo measurements with pump−probe vibrational energy relaxation measurements, the dynamical contributions to a vibrational transition can be elucidated.[16]

The echo technique was originally developed as the spin echo in magnetic resonance in 1950.[24] In 1964, the method was extended to the visible optical regime as the photon echo.[25,26] Since then, photon echoes have been used extensively to study electronic excited-state dynamics in many condensed matter systems. Previous optical coherence experiments performed on proteins examined the dephasing of electronic transitions.[27] Because of the rapid dephasing (broad homogeneous line widths) of electronic transitions, these experiments are performed only at very low temperatures, <20 K. The vibrational echo experiments enable the use of optical coherence methods to study protein dynamics at physiologically relevant temperatures.[17] Further, vibrational echoes probe dynamics on the ground-state potential surface only. Recently, vibrational echoes have been used to examine vibrational dynamics in liquids, glasses,[16,23] and proteins.[17]

The vibrational echo experiment uses a two-pulse excitation sequence. The first pulse excites a coherent superposition of the $v = 0$ and $v = 1$ vibrational levels. Immediately after the first pulse, the vibrational dipoles oscillate in phase. Because there is an inhomogeneous distribution of vibrational transition frequencies, the individual dipoles oscillate with some distribution of frequencies. Thus, the initial phase relationship is rapidly lost. This effect is the vibrational free induction decay. After a time τ, a second pulse, traveling along a path making an angle θ with that of the first pulse, excites the sample. This second pulse changes the phase factors of each vibrational superposition state in a manner that initiates a rephasing process. At time 2τ, the sample emits a third coherent pulse of light. The emitted pulse propagates along a path that makes an angle 2θ with the path of the first pulse. The third pulse is the vibrational echo. It is generated when the ensemble of microscopic dipoles is rephased at time 2τ.

The rephasing at 2τ has removed the effects of the inhomogeneous broadening. However, fluctuations of the environment that are coupled to the CO vibration cause the frequencies to fluctuate. Thus, at 2τ, the rephasing is not perfect. As τ is increased, the fluctuations produce larger accumulated phase errors among the microscopic dipoles, and the intensity of the echo is reduced. A measurement of the echo intensity versus τ is called an echo decay curve. The vibrational echo decay signal, $S(\tau)$, is given by

$$S(\tau) = S_0 e^{-4\tau/T_2} \tag{2}$$

where T_2 is the homogeneous dephasing time. The Fourier transform of the echo decay is directly related to the homogeneous line shape.[28] An exponential vibrational echo decay corresponds to a Lorentzian line shape with a width, Γ, given by

$$\Gamma = \frac{1}{\pi T_2} = \frac{1}{\pi T_2^*} + \frac{1}{2\pi T_1} \tag{3}$$

T_2 is the homogeneous dephasing time determined from the echo decay constant. T_1 is the vibrational lifetime determined from the pump−probe experiments. Measurements of T_2 and T_1 permit the determination of T_2^*, the pure dephasing contribution to the line width. In liquids, there is an additional contribution from orientational relaxation.[23] However, in the experiments presented below, orientational relaxation does not occur on the

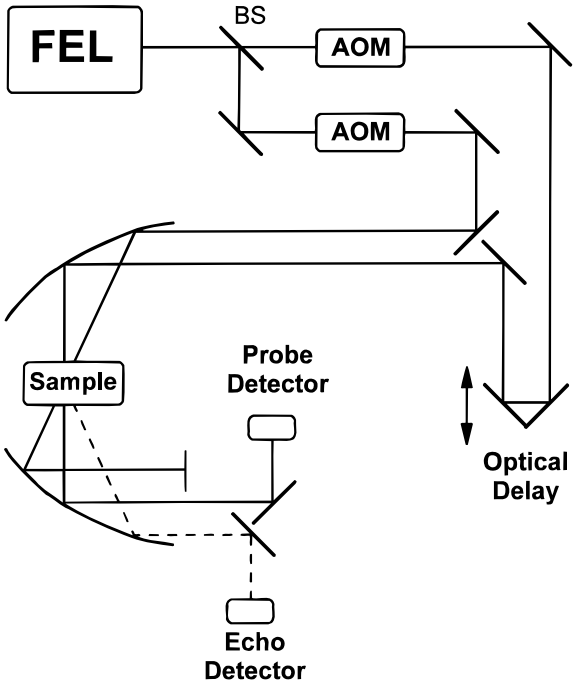

Figure 2. Schematic of the experimental apparatus used to perform the vibrational echo and pump−probe experiments. AOM denotes Ge acousto-optic modulators used as pulse selectors. BS denotes beam splitter. The dotted line indicates the path of the echo signal emitted by the sample. The differences between the two setups involves the choice of beam splitter (50% R for echo, 10% R for pump−probe), the optical pulse sequence selected by the AOMs, and in the detectors.

time scale of the experiments due to the large protein size and the solvent's high viscosity. This fact was confirmed with polarization-selective pump−probe experiments.

The vibrational echo and pump−probe experiments were performed at the Stanford Free Electron Laser (FEL) Center. The FEL pulse train consists of a macropulse having a duration of ∼3 ms and repeating at 10 Hz. Within each macropulse is a series of micropulses repeating at 11.8 MHz. Each nearly transform limited Gaussian micropulse had an energy of ∼1 μJ. The pulse duration was ∼1.7 ps for the experiments. The FEL frequency, tuned to 1969 cm^{-1} for the experiments, is actively stabilized to within 0.02% of the center frequency. Both the autocorrelation and the spectrum were monitored continuously during experiments.

A schematic of the experimental apparatus used for the vibrational echo and pump−probe experiments is shown in Figure 2. The optical beam is split into two equal parts to become the two input pulses in the vibrational echo sequence. To reduce sample heating while retaining high peak power, single micropulses are selected from the macropulse at a reduced repetition rate using germanium acousto-optic modulators (AOM). One pulse is chopped at 60 kHz, while the other is chopped at 30 kHz by a second AOM and sent through a motorized optical delay line. The chopping is performed to do background subtraction. The two beams are subsequently focused to ∼100 μm diameter spots in the sample using off-axis paraboloidal mirrors. For the experiments described here, the maximum energies of the two pulses at the sample were ∼250 and ∼150 nJ. A liquid nitrogen cooled InSb detector is used to detect the echo signal. The entire apparatus is contained in a nitrogen purge box to remove the effects of atmospheric water absorption.

The apparatus used for the pump−probe vibrational lifetime measurements is nearly identical with that used for the vibrational echo. Unlike the zero-background vibrational echo experiment, the pump−probe experiment requires accurate measurements of small changes in the probe amplitude. For this reason, 10% of the optical beam is sent into the probe AOM which selects two adjacent micropulses, instead of just one. These two pulses are highly correlated in amplitude due to the relatively high Q (30) of the FEL cavity. The remainder of the beam traveled down the delay line and through the pump AOM, which selects a single pulse. The pump and probe are crossed in the sample. A fast, liquid nitrogen cooled MMT detector was used to individually detect the two micropulses of the probe beam. The amplitude of the first of the two probe pulses, which arrives prior to the pump pulse, is used as a reference for the probe pulse (the second pulse). The signals from probe and reference are subtracted, and the results were recorded as a function of pump delay time.

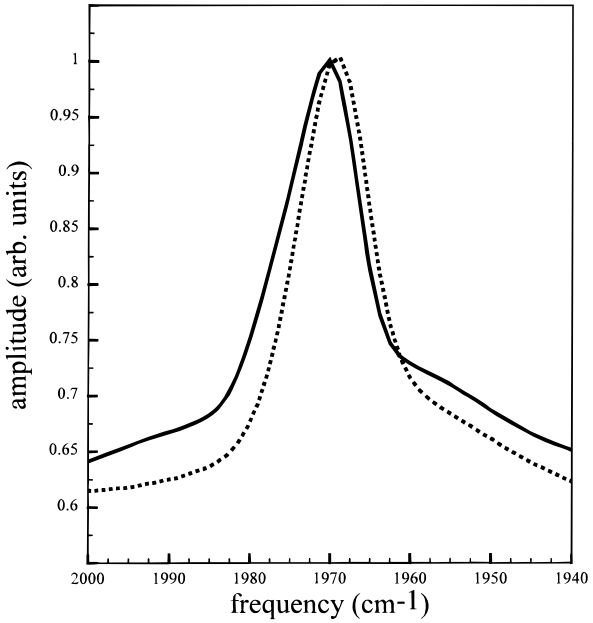

Figure 3. Mid-IR spectrum of H64V-CO in glycerol/water at 60 (dashed line) and 300 K (solid line).

At the maximum applied power, at low temperature (long T_2), the echo decays were nonexponential at short times because of the optical density effect[29] which occurs if there is significant bleaching of the absorption. An additional decay component reflecting the bleach decay is caused by vibrational lifetime relaxation. At high temperatures, the pure dephasing is so fast that there is essentially no change in the magnitude of the bleach during the echo decay. To avoid the optical density effect at all temperatures, the power was reduced until the decays were exponential. The long-time portion of the high-power decays gave the same decay constant as the low-power decays. The experiments that gave rise to the data used here were conducted with ∼65 and ∼38 nJ pulses.

The H64V sample[30] was prepared as follows: 144 mg of H64V lyophilized powder was slowly added, over a period of 2 h, to 0.45 mL of pure glycerol. After 24 h of stirring under CO, 50 μL of saturated sodium dithionite solution in 0.1 M pH 7 phosphate buffer was added to reduce the Fe. The sample cell consisting of a holder for CaF_2 flats separated by a 125 μm thick spacer was charged with 1−2 drops of the resulting solution. The sample was cooled with a helium flow cryostat. The temperature could be measured within 0.2 K.

Results

Figure 3 displays IR spectra of H64V-CO in the vicinity of the CO vibrational absorption, taken at 60 and 300 K with 2 cm^{-1} resolution. The maximum of each spectrum has been

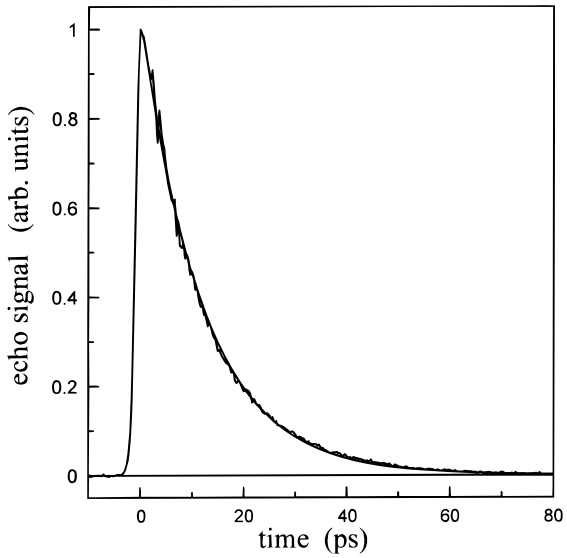

Figure 4. Vibrational echo data on H64V-CO in glycerol/water, at 60 K. The line through the data is a fit to a single-exponential decay. An exponential echo decay indicates that the homogeneous line shape is Lorentzian. At 60 K, the vibrational echo data give a value for the dephasing time constant, $T_2 = 49$ ps. Therefore, the homogeneous line width is 6.5 GHz (0.2 cm^{-1}). This is a factor of ~50 narrower than the inhomogeneously broadened absorption spectrum line width.

normalized for comparison purposes. Although there is a small shift in the peak position, the spectra appear very similar at low and high temperatures. In H64V-CO at room temperature, there is a slight shoulder to the red of the main peak, centered at about 1955 cm^{-1}. We believe that this absorption is another conformer that is made visible in these samples because of the solvent used. High glycerol concentrations appear to accentuate the lower probability conformers.[17] Other H64 mutants, e.g., H64M, have more than one conformer.[31]

Figure 4 shows an echo decay taken at 60 K. It can be seen that the signal-to-noise ratio is excellent despite the small 0.5 OD on a 0.6 OD background absorption of the protein and solvent. The line through the data is a fit to a single-exponential decay. The data is a good fit to a single exponential. Therefore, within experimental uncertainty, the homogeneous line shape is Lorentzian. The echo decays observed at all temperatures are exponential. The T_2 obtained from the 60 K data is 49 ps, yielding a homogeneous line width of 0.2 cm^{-1}. At this temperature, the width of the absorption spectrum is 11.7 cm^{-1}. Thus, the line is massively inhomogeneously broadened, the two widths differing by a factor of ~58.

The temperature dependence of the vibrational echo decays as well as the pump−probe lifetime measurements were obtained from 60 to 300 K. Each decay was fit to a single exponential. For the high-temperature echo decays, the decay times are approaching the pulse width. Therefore, the data were fit to the convolution of a Gaussian instrument response and an exponential. (This is an approximate method for performing the convolution in an echo experiment, but it is sufficiently accurate in the present case, where the decays are not too fast.) Care was taken in each case to verify the stability of the fit, and for most temperatures, the decay constant could be determined within 3% for the echo data and 5% for the pump−probe data. At temperatures below 60 K, the homogeneous dephasing rate is dominated by the lifetime to such an extent that it is not possible to obtain the pure dephasing times accurately.

Figure 5 shows temperature-dependent data. The triangles are the measured values of T_2 obtained from the vibrational echo decays using eq 2. The circles are $2T_1$. T_1 is the decay constant measured in the pump−probe vibrational lifetime experiment. From eq 3, it is seen that the relevant quantity is twice the lifetime, or $2T_1$. The squares are T_2*, the pure dephasing time, obtained from T_2 and $2T_1$, using eq 3. T_1 has a mild temperature dependence. T_2 has a steeper temperature dependence, changing by a factor of about 8 between 60 and 300 K. The pure dephasing, T_2*, which arises from the vibrational energy level fluctuations, has a steep temperature dependence. At the lowest temperatures, the lifetime is the major contributor to the homogeneous dephasing (inverse of the line width). By room temperature, the lifetime contribution to the homogeneous line is small; the pure dephasing completely dominates the homogeneous dephasing. At all temperatures, the line is inhomogeneously broadened. At room temperature, the homogeneous line width is 1.9 cm^{-1} while the absorption spectrum fwhm width is ~12 cm^{-1}, i.e., the absorption spectrum is about 6 times wider than the homogeneous line width.

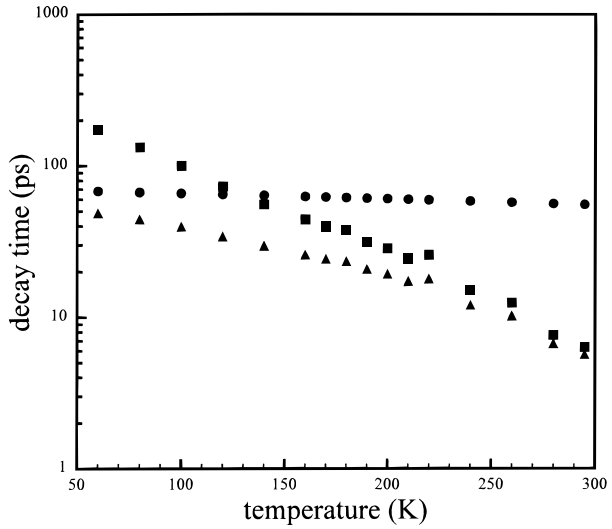

Figure 5. Temperature-dependent data. The triangles are the measured values of T_2 obtained from the vibrational echo decays using eq 2. The circles are $2T_1$. T_1 is the decay constant measured in the pump−probe vibrational lifetime experiments. The squares are T_2*, the pure dephasing time, obtained from T_2 and $2T_1$, using eq 3.

Calculations show that the 300 K absorption spectrum (Figure 3) fits well to a convolution of the 1.9 cm^{-1} Lorentzian homogeneous line width as obtained from the vibrational echo experiment and the 11.7 cm^{-1} Gaussian inhomogeneous line width obtained from the 60 K spectrum. This suggests that the inhomogeneous spectrum remains essentially unchanged from low temperature to room temperature. The room-temperature spectrum is the convolution of the inhomogeneous and homogeneous lines. This type of analysis was not possible on Mb due to the difficulty in obtaining a clean A_1 transition spectrum at room temperature with the A_0, A_2, and A_3 transitions nearby. Spectra show that these peaks shift slightly in frequency and relative amplitude with temperature, causing the 300 K spectrum to appear broader than that calculated by convolving the low-temperature inhomogeneous absorption line width and the room-temperature homogeneous width.

Observation of a photon echo decay in which $1/\pi T_2$ is much less than the spectroscopic line width demonstrates that the line is inhomogeneously broadened. On the time scale of the echo decay there is an essentially static component of the absorption line. In a mix crystal, the static part arises from crystal defects and strains, and the dynamics responsible for the homogeneous dephasing arise from thermally populated phonons. In a crystal, particularly at low temperature, the static part can be truly time

independent. In a glass, there is a broad distribution of time scales associated with the evolution of the nonequilibrium glassy structure.[32] Even at low temperature (1 K), structural dynamics can range from 10^{-12} to 10^{7} s and longer. In a glass, dynamics that are slow compared to the homogeneous dephasing time provide the inhomogeneous broadening that is removed by the echo experiment. Unlike a crystal, the inhomogeneous broadening in a glassy system is not caused by a completely static structure. The situation in a protein is analogous to that in a glass. An ensemble of Mb-CO's contains proteins with many slightly different structures that can interconvert. At room temperature, presumably all possible structures are sampled on some time scale. There is a broad distribution for the rates of structural fluctuations, and, therefore, a broad distribution of rates of the Mb-CO vibrational energy fluctuations. The structures, which interconvert on times scales slow compared to the homogeneous dephasing time, give rise to the inhomogeneous broadening. The mechanism for the homogeneous dephasing has been discussed previously,[17] and it is discussed further below. Protein structural fluctuations produce fluctuating electric fields. These fluctuating electric fields couple to the heme and cause fluctuations in the back donation of electron density to the CO π^* antibonding molecular orbital. The inhomogeneous broadening of the CO transition is caused by the inhomogeneous distribution of electric fields, which evolve on a time scale slow compared to the homogenous dephasing time, experienced by the ensemble of heme-CO's. This picture is supported by experiments that show the A_0-A_3 band splittings arise from differences in electric fields produced by the four conformations of the distal histidine.[3]

The observation of the inhomogeneous broadening at room temperature indicates that, on the echo time scale, the protein exists in many distinguishable conformational substates that induce different transition frequencies of the carbonyl stretch. The FEL was tuned ± 4 cm^{-1} around the peak of the spectrum. The time dependences of the vibrational echo decays and the pump−probe decays were unchanged by these shifts in wavelength, demonstrating that the dynamics are independent of the position in the inhomogeneous line over this range of wavelengths.

Figure 6 displays the mutant H64V-CO pure dephasing rate, $1/T_2^*$, on a log plot. The temperature dependence of the pure dephasing rate is much milder at low temperatures, with a break in the dependence at ~185 K, the approximate glass transition temperature of the solvent. The data fit well to eq 1. The low-temperature data fall on a straight line, suggesting that the temperature dependence can be described by a power law, T^{α}. The exponent of the power law is $\alpha = 1.3 \pm 0.1$ for H64V-CO. This value of α should be compared to the Mb data, which also give $\alpha = 1.3 \pm 0.1$.[17] Within experimental error, the exponents are identical.

To find the activation energy, there are two ways to obtain a fit, and they yield somewhat different activation energies but the same power law exponent. One method is to assume that both terms in eq 1 are active at all temperatures, while the other assumes a change in mechanism at the solvent's glass transition. If eq 1 is used as written, i.e., the sum of the two functions, $\Delta E = 1250$ cm^{-1}. The activated process makes little contribution at the lower temperatures. However, the power law contributes 25% at room temperature. In the second approach, at low temperature, the dephasing is given only by the power law. This does not change the value of α. At the glass transition, the dephasing becomes only exponentially activated. Therefore, there is no contribution from the power law at high temperature. Using this approach, the activated process fits the data with

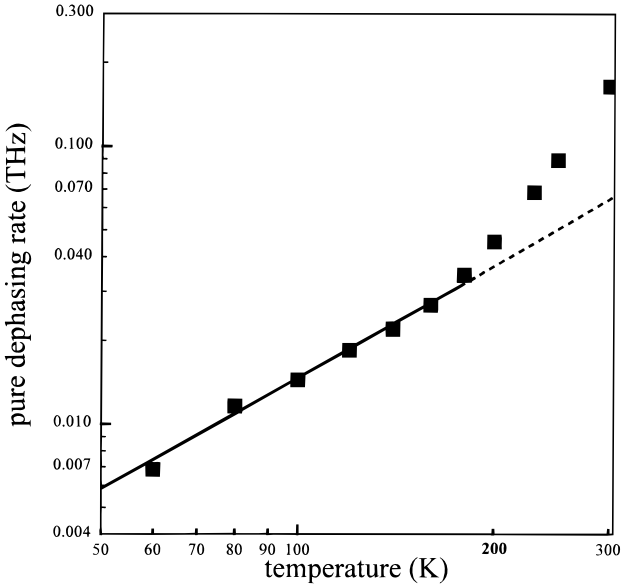

Figure 6. log plot of the pure dephasing rate, $1/T_2^*$, versus temperature for H64V-CO. Below the solvent's glass transition temperature, the data follow a power law, $T^{1.3}$, dependence, which appears linear on the log plot. Above ~185 K, an exponentially activated process describes the data with $\Delta E = \sim 1000$ cm^{-1}.

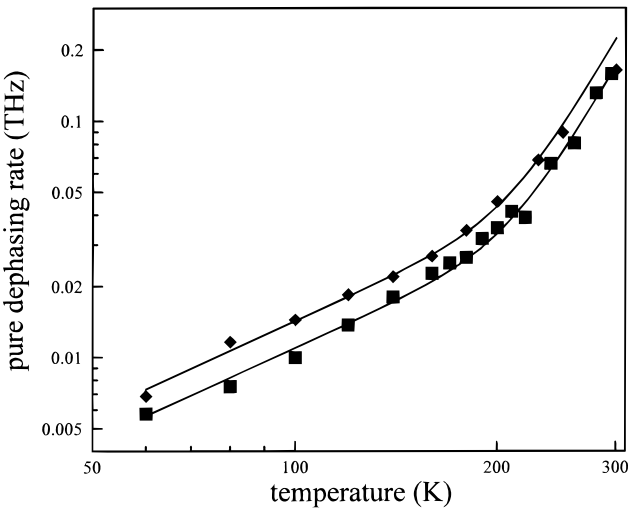

Figure 7. log plot of the pure dephasing rate, $1/T_2^*$, versus temperature for H64V-CO (squares) and Mb-CO (diamonds). The room-temperature point of the Mb data has a large error bar. The solid line through the H64V-CO data was translated up to form the solid line through the Mb-CO data. No other change in the line was made. A vertical translation on a log plot is the equivalent of multiplying a function by a constant. This demonstrates that the two data sets have the identical functional form of the temperature dependence within experimental error.

$\Delta E = 800$ cm^{-1}. Both of these values are the same as those found for Mb-CO.[17] As with Mb-CO it is unclear which of these models is correct. It needs to be emphasized that while eq 3 fits the data extremely well, it cannot be proven to be unique. The important point is that the functional forms of the data and the α and ΔE values for the mutant Mb and the wild-type Mb are identical within experimental error.

Figure 7 compares the data for the mutant H64V-CO and Mb-CO. The dephasing rate for H64V-CO is slower than for Mb over the entire temperature range. At room temperature, the Mb point has a very large error bar. Comparing the data points at each temperature reveals that the H64V-CO data is 21% ± 3% slower than the Mb data with no systematic variation. A solid line is drawn through the H64V-CO data. It

was obtained from a fit of eq 3 to the data. This line was translated up with no change in shape or scale and is the line through the Mb-CO data. The translation on the log plot is the same as multiplying the function that passes through the H64V-CO by a constant. It can be seen that within experimental error, the functional form of the two data sets is identical.

Kinetic and thermodynamic evidence has been reported to suggest that the mutant is functionally different than Mb. For example, the spontaneous thermal dissociation constant of CO is approximately 2.5 times faster in the mutant. Also, the CO affinity of the mutant is 5 times faster than Mb.[33] Thus, the single point mutation, which has a significant effect on the protein function, also influences the Mb-CO vibrational dynamics.

Discussion

In the previous papers on wild-type Mb-CO,[17,18] it was argued that the motions of the solvent, glycerol/water, were not responsible for the dephasing. For the solvent to cause dephasing, its motions must couple to the transition frequency of the CO. When molecules go from the gas phase to a condensed phase, there is a shift of electronic and vibrational transition frequencies. This effect is referred to as the solvent shift. Molecular interactions with the condensed matter environment are responsible for line broadening as well as the solvent shift. These phenomena are closely related. The line broadening can be static, giving rise to an inhomogeneous line, or dynamic, giving rise to a homogeneous line. In either case, it is the variations in the solvent shift that cause line broadening.

In Mb-CO, the nature of the solvent itself has little effect on the CO vibrational transition frequency. The Mb-CO transition frequency is virtually identical in a wide variety of liquids and glasses.[2,34,35] The solvent shift is unaffected by the medium surrounding the protein even when the change is from a liquid solvent such as water or a mixture of glycerol/water to a protein crystal.[35] In contrast, the frequency difference between the A_0 and A_1 lines in Mb-CO is 24 cm^{-1}.[2] This difference is caused by a change in conformation of the protein, especially the distal histidine. Changes in the protein structure can have a major influence on the CO vibrational frequency while changes in the solvent have a negligible influence. This spectroscopic information leads to the reasonable conclusion that fluctuations of the protein structure will cause homogeneous dephasing while fluctuations of the solvent structure will not. The solvent does provide a heat bath and a boundary condition that are intimately involved in the protein fluctuations and the dephasing, but the argument made above strongly supports the idea that the dephasing does not arise from direct coupling of the solvent dynamics to the CO transition frequency.

In the H64V-CO experiments, everything about the protein pocket and the experimental procedures is the same as in the previous Mb experiments except for the substitution of the distal histidine by a valine. This amino acid change causes an ~20% reduction in the pure dephasing rate. Thus, a change in the structure of the pocket produces a change in the coupling of the protein fluctuations to the CO ligand bound at the active site. These results confirm that CO pure dephasing is caused by coupling to the protein fluctuations since a change in the protein with no change in the solvent produces a substantial change in the rate of pure dephasing.

H64V-CO is a mutant of wild-type sperm whale myoglobin. The vibrational echo results presented here are compared to the previous vibrational echo results on horse heart myoglobin. It is necessary to consider whether this difference matters. Sperm whale myoglobin (not the mutant) and horse heart myoglobin differ only in a small number of amino acids sites. These sites are well removed from the protein pocket. There is no difference between sperm whale and horse heart myoglobin in the frequency of the A1 absorption peak.[36] This demonstrates that the small differences in the amino acid sequence well removed from the pocket does not change the coupling of the protein to the CO ligand bound at the active site. Furthermore, measurements of the vibrational lifetimes of CO bound to sperm whale and horse heart myoglobin give identical results.[36] This dynamical measurement lends addition support to the validity of comparing vibrational echo results from the H64V-CO mutant of sperm whale to those from horse heart Mb-CO.

In discussing the dephasing experiments on Mb-CO,[17] it was proposed that fluctuating electric fields produced by time-dependent protein structural fluctuations are responsible for CO vibrational dephasing. It is well established from work on Mbs and other metal carbonyls[37−40] that changes in the back donation of electron density (back bonding) into the CO π^* antibonding molecular orbital are responsible for static shifts of the CO vibrational frequency. Increased back bonding weakens the CO bond and red-shifts the vibrational frequency. In Mb-COs and CO bound to metal porphyrins, the metal d_π, nitrogen p_π, and carbon p_π electrons form a π-electron system that is delocalized across the heme (or heme-like) macrocycle. It is this delocalized d_π/p_π system that back donates electron density to the CO π^* molecular orbital. Experiments by Oldfield et al.[3] indicate that in different Mb's, variations in electric fields resulting from different protein conformations are responsible for changes in back bonding and, therefore, the observed static shifts in vibrational frequency.[40,41]

In the proposed fluctuating electric field dephasing mechanism, protein motions result in motions of the amino acids. The dynamics of these amino acids, particularly the polar ones, produce fluctuating electric fields at the heme macrocycle. The fluctuating fields generate time-dependent variations in the macrocycle's electron density distribution, which, in turn, cause time evolution of the magnitude of the back bonding. It is this time-dependent back bonding that is responsible for the CO vibrational energy fluctuations, i.e., the vibrational pure dephasing.

In the protein pocket that contains the heme-CO, there are two highly polar amino acids, the proximal histidine and the distal histidine. The distal histidine is not directly bound to the heme-CO. We have observed that replacing the polar distal histidine with the nonpolar valine residue reduces the rate of pure dephasing by ~20% but does not change the functional form of the temperature dependence. This is consistent with and provides support for the fluctuating electric field induced dephasing mechanism. The structure of the pocket differs only in a single residue. However, this difference is significant. The interaction between CO and the polar distal histidine is replaced by a weaker interaction between CO and the nonpolar valine. Other less significant structural differences, and differences in Mb affinity for CO which arise as a result of this substitution have been discussed in detail in the literature.[5,42]

X-ray crystallographic data of this mutant show the equilibrium structure of the protein is not significantly different from that of myoglobin.[5] Therefore, it is unlikely that there is a significant change in the global dynamics of the protein. Thus, the temperature dependence of the CO vibrational pure dephasing is unchanged since it reflects the spectrum of protein fluctuations that are coupled to the CO. However, the strength of the coupling of the protein fluctuations to the CO will be reduced because one of the closest sources of the fluctuating electric field has been removed.

The reduced coupling of the protein to the heme is also evidenced by the change in the CO vibrational frequency in H64V compared to the dominant A_1 line of Mb. The A_1 line of Mb is at 1945 cm^{-1}, while the H64V line is at 1969 cm^{-1}. The higher frequency is caused by less back bonding. In previous studies of the vibrational lifetimes of Mbs and model heme compounds, it was found that there was a direct correlation between the CO absorption frequency and the lifetime.[36,43−45] Higher vibrational transition frequency was linearly associated with a longer vibrational lifetime. This demonstrated that the vibrational lifetime was determined by coupling to the heme π-electron system via the back-bonding interaction. Increased back bonding caused by stronger electric field interactions with the protein results in a shift of the absorption to lower energy and a shorter vibrational lifetime. In the current experiments, the CO stretch frequency of H64V-CO absorbs at higher frequency than the Mb A_1 line because of a decrease in the electric field induced back bonding. The reduction in static coupling is associated with weaker coupling of the protein fluctuations to the heme macrocycle and thus to the slower dephasing in H64V-CO observed in these vibrational echo experiments.

The CO vibrational frequency of H64V-CO and the A_0 line of Mb-CO are almost identical. The CO vibrational lifetimes at room temperature of H64V-CO and A_0 of Mb-CO are 27 and 26 ps, respectively. These are identical within experimental error, consistent with the previous studies of the relationship between the CO frequency and the vibrational lifetime. An interesting question arises: will the vibrational dephasing of H64V and A_0 be almost identical? In future experiments, it may be possible to perform vibrational echo experiments on the A_0 line of Mb. However, such experiments may be more difficult than the studies presented here because the A_0 line is a relatively small shoulder on the larger A_1 line.

In the absence of the distal histidine in H64V-CO, pure dephasing can still occur because of the motions of the proximal histidine and fluctuation of the more distant parts of the protein. The proximal histidine may play a unique role in the dephasing because it is the only covalent link between the heme and the protein. Motions of the Fe and the protein are coupled through the proximal histidine.[1] Therefore, in addition to an electric field effect, the proximal histidine motions may produce a "mechanical" contribution to the pure dephasing.[17] The roles of the proximal amino acids will be examined in future experiments.

The temperature dependence observed for H64V-CO is the same as that discussed in considerable detail previously.[17] While the CO pure dephasing is not caused by direct coupling of the CO to the solvent dynamics, the solvent still plays a significant role. Below the solvent T_g, the glycerol/water glass imposes a rigid boundary condition on the protein surface topology. Protein motions are restricted to those that do not much change the surface topology. This gives rise to the apparent $T^{1.3}$ power law temperature dependence. The $T^{1.3}$ temperature dependence can arise from tunneling dynamics of a system of protein two-level systems (PTLS).[17] The PTLS are akin to the two level systems of very low temperature glasses. The same statistical mechanics machinery used to describe the low temperature ($\sim$1 K) heat capacities of glasses[46,47] and the optical dephasing of electronic transitions of chromophores in low-temperature glasses[32] can be used to describe the PTLS-induced vibrational dephasing of Mb-CO at much higher temperatures ($\sim$100 K). It needs to be stressed that other physical processes can yield similar temperature dependences. For example, a power law temperature dependence can arise from activation over barriers rather than tunneling if there is the appropriate broad distribution of activation energies. In either case, the results indicate the existence of a complex protein energy landscape.

Above the solvent T_g, the solvent boundary with the protein is no longer rigid. The protein can now undergo structural fluctuations that involved surface shape changes. The temperature dependence is an activated process. In addition to the change in temperature, the reduction in the solvent viscosity with increasing temperature may play an important role in the temperature dependence of the CO vibrational dephasing. The viscosity dependence at fixed temperature of the vibrational dephasing is currently under investigation.

Concluding Remarks

In this paper, we have extended the application of vibrational echoes to mutant proteins. The vibrational echo experiments provide a method for the removal of the inhomogeneous broadening from a vibrational spectrum yielding the dynamical information contained in the homogeneous spectrum. We have performed vibrational echo and lifetime relaxation measurements on CO bound to the active site of H64V, a mutant of myoglobin with the distal histidine replaced with a valine. Combining the results of the echo with pump−probe data, we have obtained the pure dephasing times, T_2*, at a series of temperatures from 60 to 300 K. T_2* is a measure of the vibrational energy level fluctuations induced by conformational fluctuations of the protein. It is found that the H64V-CO vibrational line is inhomogeneously broadened at all temperatures in this range. Thus, even at room temperature, the ensemble of protein molecules exists in a distribution of conformational substates that interconvert slowly compared to the 10 ps time scale of the echo experiment.

The general mechanism proposed previously[17] to explain the coupling of conformational fluctuations of the protein to the vibrational transition energy to cause pure dephasing is supported by this work. It is known that static changes in heme back bonding to the CO antibonding π* molecular orbital result in changes in the transition energy of the CO vibration. It was proposed that protein conformational fluctuations cause fluctuations in the back bonding and, therefore, cause pure dephasing.[17] The model stated that protein motions produce fluctuating electric fields which give rise to the time-dependent back bonding. Replacing the polar distal histidine with the nonpolar valine removes one source of the fluctuating electric fields, thus reducing the coupling between the protein fluctuations and the measured pure dephasing. The observation that the rate of pure dephasing observed in H64V-CO is reduced significantly compared to Mb-CO is consistent with the model. The picture that emerges is that the heme acts as an antenna that receives and communicates protein fluctuations to the vibration of the CO ligand bound at the active site.

Acknowledgment. This research was supported by the Medical Free Electron Laser Program, through the Office of Naval Research (N00014-94-1-1024) (C.W.R., M.D.F., A.K.). Additional support was provided by the National Science Foundation, Division of Materials Research (DMR93-22504) (K.D.R., M.D.F.), the Office of Naval Research, Biology Division, (N00014-95-1-0259) and the National Science Foundation, Division of Materials Research (DMR94-04906) (D.D.D., J.R.H.) and the National Institutes of Health (PHSRO1 GM-31756, PHSRO1 GM-33775) (S.G.S., E.C.).

References and Notes

(1) Stryer, L. *Biochemistry*, 3rd ed.; W. H. Freeman and Co.: New York, 1988.

(2))Ansari, A.; Beredzen, J.; Braunstein, D.; Cowen, B. R.; Frauenfelder, H.; Hong, M. K.; Iben, I. E. T.; Johnson, J. B.; Ormos, P.; Sauke, T.; Schroll, R.; Schulte, A.; Steinback, P. J.; Vittitow, J.; Young, R. D. *Biophys. Chem.* **1987**, *26*, 337.

(3) Oldfield, E.; Guo, K.; Augspurger, J. D.; Dykstra, C. E. *J. Am. Chem. Soc.* **1991**, *113*, 7537.

(4) Kuriyan, J. W.; Karplus, M.; Petsko, G. A. *J. Mol. Biol.* **1986**, *192*, 133.

(5) Quillin, M. L.; Arduini, R. M.; Olson, J. S.; Phillips, G. N., Jr. *J. Mol. Biol.* **1993**, *234*, 140.

(6) DeBrunner, P. G.; Franuenfelder, H. *Ann. Rev. Phys. Chem.* **1982**, *33*, 283.

(7) Frauenfelder, H.; Parak, F.; Young, R. D. *Annu. Rev. Biophys. Biophys. Chem.* **1988**, *17*, 471.

(8) Owrutsky, J. C.; Li, M.; Locke, B.; Hochstrasser, R. M. *J. Phys. Chem.* **1995**, *99*, 4842.

(9) Jackson, T. A.; Lim, M.; Anfinrud, P. A. *Chem. Phys.* **1994**, *180*, 131.

(10) Petrich, J. W.; Martin, J. L. . In *Time-Resolved Spectroscopy*; Clark, R. J. H., Hester, R. E., Eds.; Wiley: New York, 1989; p 335.

(11) Friedman, J. M.; Rousseau, D. L.; Ondrias, M. R. *Annu. Rev. Phys. Chem.* **1982**, *33*, 471.

(12) Alben, J. O.; Caughy, W. S. *Biochemistry* **1968**, *7*, 175.

(13) Alben, J. O.; Beece, D.; Browne, S. F.; Doster, W.; Eisenstein, L.; Frauenfelder, H.; Good, D.; McDonald, J. D.; Marden, M. C.; Moh, P. P.; Reinisch, L.; Reynolds, A. H.; Shyamsunder, E.; Yue, K. T. *Proc. Natl. Acad. Sci. U.S.A.* **1982**, *79*, 3744.

(14) Elber, R.; Karplus, M. *Science* **1987**, *235*, 318.

(15) Iben, I. E. T.; Basunstein, D.; Doster, W.; Frauenfelder, H.; Hong, M. K.; Johnson, J. B.; Luck, S.; Ormos, P.; Schulte, A.; Steinback, P. J.; Xie, A.; Young, R. D. *Phys. Rev. Lett.* **1989**, *62*, 1916.

(16) Tokmakoff, A.; Zimdars, D.; Urdahl, R. S.; Francis, R. S.; Kwok, A. S.; Fayer, M. D. *J. Phys. Chem.* **1995**, *99*, 13310.

(17) Rella, C. W.; Rector, K.; Kwok, A.; Hill, J. R.; Schwettman, H. A.; Dlott, D. D.; Fayer, M. D. *J. Phys. Chem.* **1996**, *100*, 15620.

(18) Rella, C. W.; Kwok, A.; Rector, K. D.; Hill, J. R.; Schwettmann, H. A.; Dlott, D. D.; Fayer, M. D. *Phys. Rev. Lett.* **1996**, *77*, 1648.

(19) Gordon, R. G. *J. Chem. Phys.* **1965**, *43*, 1307.

(20) Gordon, R. G. *Adv. Magn. Reson.* **1968**, *3*, 1.

(21) Berne, B. J. *Physical Chemistry: An Advanced Treatise*; Academic Press: New York, 1971; Vol. VIIIB.

(22) Loring, R. F.; Mukamel, S. *J. Chem. Phys.* **1985**, *83*, 2116.

(23) Tokmakoff, A.; Fayer, M. D. *J. Chem. Phys.* **1995**, *102*, 2810.

(24) Hahn, E. L. *Phys. Rev.* **1950**, *80*, 580.

(25) Kurnit, N. A.; Abella, I. D.; Hartmann, S. R. *Phys Rev. Lett.* **1964**, *13*, 567.

(26) Abella, I. D.; Kurnit, N. A.; Hartmann, S. R. *Phys. Rev. Lett.* **1966**, *14*, 391.

(27) Leeson, D. T.; Wiersma, D. A. *Phys. Rev. Lett.* **1995**, *74*, 2138.

(28) Farrar, T. C.; Becker, D. E. *Pulse and Fourier Transform NMR*; Academic Press: New York, 1971.

(29) Olson, R. W.; Lee, H. W. H.; Patterson, F. G.; Fayer, M. D. *J. Chem. Phys.* **1982**, *76*, 31.

(30) Springer, B. A.; Sligar, S. G. *Proc. Natl. Acad. Sci. U.S.A.* **1987**, *84*, 8961.

(31) Braunstein, D. P.; Chu, K.; Egeberg, K. D.; Frauenfelder, H.; Mourant, J. R.; Nienhaus, G. U.; Ormos, P.; Sligar, S. G.; Springer, B. A.; Young, R. D. *Biophys. J.* **1993**, *65*, 2447.

(32) Narasimhan, L. R.; Littau, K. A.; Pack, D. W.; Bai, Y. S.; Elschner, A.; Fayer, M. D. *Chem. Rev.* **1990**, *90*, 439.

(33) Springer, B. A.; Egeberg, K. D.; Sligar, S. G.; Rohlfs, R. J.; Mathews, A. J.; Olson, J. S. *J. Biol. Chem.* **1988**, *264*, 3057.

(34) Hill, J. R.; Dlott, D. D.; Fayer, M. D., unpublished results, 1996.

(35) Ivanov, D.; Sage, J. T.; Keim, M.; Powell, J. R.; Asher, S. A.; Champion, P. M. *J. Am. Chem. Soc.* **1994**, *116*, 4139.

(36) Hill, J. R.; Dlott, D. D.; Rella, C. W.; Peterson, K. A.; Decatur, S. M.; Boxer, S. G.; Fayer, M. D. *J . Phys. Chem.* **1996**, *100*, 12100.

(37) Cotton, F. A.; Wilkinson, G. *Advanced Inorganic Chemistry*; Wiley-Interscience: New York, 1988.

(38) Boldt, N. J.; Goodwill , K. E.; Bocian, D. F. *Inorg. Chem.* **1988**, *27*, 1188.

(39) Spiro, T. G. *Iron Porphyrins*; Addison-Wesley: Reading, MA, 1983; Vol. II.

(40) Li, X. Y.; Spiro, T. G. *J. Am. Chem. Soc.* **1988**, *110*, 6024.

(41) Park, K. D.; Guo, K.; Adebodun , F.; Chiu, M. L.; Sligar, S. G.; Oldfield, E. *Biochemistry* **1991**, *30*, 2333.

(42) Springer, B. A.; Sligar, S. G.; Olson, J. S.; Phillips, G. N., Jr. *Chem. Rev.* **1994**, *94*, 699.

(43) Dlott, D. D.; Fayer, M. D.; Hill, J. R.; Rella, C. W.; Suslick, K. S.; Ziegler, C. J. *J. Am. Chem. Soc.* **1996**, *118*, 7853.

(44) Hill, J. R.; Dlott, D. D.; Fayer, M. D.; Rella, C. W.; Rosenblatt, M. M.; Suslick, K. S.; Ziegler, C. J. *J. Phys. Chem.* **1996**, *100*, 218.

(45) Hill, J. R.; Rosenblatt, M. M.; Ziegler, C. J.; Suslick, K. S.; Dlott, D. D.; Rella, C. W.; Fayer, M. D. *J. Phys. Chem.* **1996**, *100*, 18023.

(46) Phillips, W. A. *Amorphous Solids. Low Temperature Properties, Topics in Current Physics*; Springer: Berlin, 1981.

(47) Stevels, J. M. The Structural and Physical Properties of Glass. In *Thermodynamcis of Liquids and Solids*; Flügge, S., Ed.; Springer-Verlag: Berlin, 1962; p 13.

(48) Yang, F.; Phillips, G. N. *J. Mol. Biol.* **1996**, *256*, 762.